

Spin Generation Via Bulk Spin Current in Three Dimensional Topological Insulators

Xingyue Peng¹, Yiming Yang¹, Rajiv R. P. Singh¹, Sergey Y. Savrasov¹ and Dong Yu^{1,2}

July 19, 2022

Abstract

To date, spin generation in three-dimensional topological insulators (3D TIs) is primarily modeled as a single-surface phenomenon, happening independently on top and bottom surfaces. Because this surface charge transport is Boltzmann-like, the surface spin accumulation is expected to be proportional to the momentum relaxation time or the inverse of the impurity density. Here we propose a fundamentally new mechanism for spin generation based on the topological nature of the band structure: an external electric field creates a transverse pure spin current in the bulk of 3D TIs, which transports spins between the top and bottom surfaces and leads to spin accumulation on both. The surface spin density and charge current are then proportional to the spin relaxation time, which can be extended by nonmagnetic scattering via the Dyakonov-Perel spin relaxation mechanism. Therefore, this new spin generation mechanism results in a distinct strategy for the enhancement of surface spin polarization by extending the spin relaxation time through increasing the impurity density. Since this efficient spin generation directly originates from the unique band topology of the TIs, it does not exist in other two-dimensional (2D) systems such as graphene and two-dimensional electron gas (2DEG). This theory is supported by the experimental observation of high conductivity near the Dirac point, which indicates large spin density at the TI surface under an external electric field even when “free carriers” are depleted.

arXiv:1410.5494v1 [cond-mat.mtrl-sci] 20 Oct 2014

¹Department of Physics, University of California, Davis, One Shields Avenue, Davis, California 95616 USA

²Email: yu@physics.ucdavis.edu

Topological insulators (TIs) have attracted world-wide attention because of their intriguing fundamental physics and exciting application opportunities in spintronics [1]. The recently-discovered three-dimensional (3D) TIs [2, 3] are of particular technological importance since the unique spin generation can be realized in single crystals rather than in complex heterogeneous structures [4]. TIs are considered as efficient spin generators [5], yet the spin generation is generally regarded as a pure surface phenomenon. Namely, the electronic momentum and spin are locked at the TI surface, and a net charge current leads to a net spin polarization at the surface, whose magnitude is directly proportional to the charge current [6]. In this view, all physics occurs independently at the top and bottom surfaces of a TI. The role of the bulk is passive and simply separates the top and bottom surfaces, and the surface conductivity of a 3D TI is similar to a normal 2D system such as graphene or 2-dimensional electron gas (2DEG), except perhaps for the dominant spin-orbit interaction. While the charge transport at the edge of a 2D TI is dissipationless [7, 4], both theories [8] and experiments [9, 10, 11, 12] show that the charge transport on a 3D TI surface is not, because charge carriers can be scattered by nonmagnetic defects to a different angle even though backscattering is forbidden. Therefore, the surface conductivity of a 3D TI is expected to be proportional to scattering time (or momentum relaxation time) τ , which is inversely proportional to the impurity density n_i .

Here we present a fundamentally different mechanism that can efficiently generate spin polarization at the surface of a 3D TI, in addition to the aforementioned surface charge current mechanism. In our view, the insulating bulk plays an essential role and acts as a bridge for transporting spins between top and bottom surfaces, in a direction perpendicular to the applied electric field. Consequently, opposite spins accumulate at the top and bottom surfaces, respectively. Thus, the spin density generated by this mechanism at the surface is proportional to the spin relaxation time τ_s , instead of τ . As frequent nonmagnetic scattering slows down the spin relaxation through the Dyakonov-Perel spin relaxation mechanism (i.e. $\tau_s \sim 1/\tau$), the spin density and the surface conductivity are then expected to be proportional to $1/\tau$ or n_i . If the defect density is high, as in practical TI materials such as Bi_2Se_3 , our spin generation mechanism via bulk spin current is likely dominant. Our theory is rigorously confirmed by calculations based upon a simple effective band model and is well supported by the experimental observations of high conductivity at the Dirac point.

We will first show the calculation results based on an effective band model to demonstrate the anomalous conductivity and associated spin generation. Then a comprehensive picture will be presented to intuitively reveal its physical origin. In this picture, the spin relaxation dynamics at the TI surface (Dyanokov-Perel mechanism) is first examined, where we find the spin relaxation time can be extended by nonmagnetic scattering. Next, the topological nature of the band structure is demonstrated, which leads to a bulk spin current and accumulates spins at the surface under an external electric field. A following comparison between the 2D surface of 3D TIs and other 2D systems, including graphene and 2DEG, is made to further clarify the importance of band topology. Finally, we will demonstrate the experimental evidence supporting this theory.

Anomalous conductivity and spin accumulation

Because the spin generation mechanism roots in the band topology rather than the detailed energy dispersion as shown later, we adopt a simplified effective band Hamiltonian to allow for an analytic solution and a clear physical picture. Consider the effective Hamiltonian on the top surface of a 3D TI

$$H_0 = \hbar v_F \boldsymbol{\sigma} \cdot \mathbf{k} \quad (1)$$

where v_F is the constant Fermi velocity, \mathbf{k} is the wave vector within the surface and $\boldsymbol{\sigma}$ is the pseudo-spin of the surface electrons. $\boldsymbol{\sigma}$ is actually the vector basis formed by 2 atomic orbitals and may have no essential relation to the real spin. In most TI materials such as Bi_2Se_3 , these two orbitals highly match the real-spin eigenstates and the pseudo-spin $\boldsymbol{\sigma}$ may be (and is often) approximately regarded as the rotated real spin $\mathbf{n} \times \boldsymbol{\sigma}_{\text{real}}$ where \mathbf{n} is the normal vector of the surface [13]. Due to the linear approximation, this Hamiltonian only works for a limited region near the Γ point (Dirac point) in k-space.

The charge current operator is then given by

$$\mathbf{j} = \frac{(-e)}{\hbar} \frac{\partial H_0}{\partial \mathbf{k}} = -e v_F \boldsymbol{\sigma} \quad (2)$$

which is directly proportional to the spin (understood as pseudo-spin, same as below unless specified).

Considering scattering U as well as a constant in-plane external electric field \mathbf{E} , the full Hamiltonian is

$$H = H_0 + e\mathbf{E} \cdot \mathbf{r} + U \quad (3)$$

where e is the charge unit, $e > 0$. As long as the system has well-defined energy bands, we may think of each scattering center as well-isolated and treat the latter two terms in the above equation as perturbations. Here we make no assumption of a low impurity density n_i , as opposed to [8]. To focus on the physical picture, we will detail the complete derivation in the Supplementary Information but directly present the major results. The total surface conductivity can be shown to have two components

$$\sigma_{xx} = \sigma_{xx}^n + \sigma_{xx}^a \quad (4)$$

where the first term σ_{xx}^n turns out to be the normal Boltzmann conductivity

$$\sigma_{xx}^n = \frac{e^2 v_F k_F \tau(k_F)}{h} \quad (5)$$

in agreement with Ref. [8].

The second term σ_{xx}^a has an expression

$$\sigma_{xx}^a = \frac{e^2 n_i}{16\pi \hbar^3 v_F^2} \left[\xi(k_F) + \int_{k_F}^{+\infty} \frac{\xi(k)}{k} dk \right] \quad (6)$$

where $\xi(k)$ is an angular integral related to the elastic scattering potential $\bar{U}_{\mathbf{k}\mathbf{k}'}$

$$\xi(k) \equiv \frac{1}{2\pi} \oint_{|\mathbf{k}'|=|k|} |\bar{U}_{\mathbf{k}\mathbf{k}'}|^2 (1 - \cos \gamma)^2 d\gamma \quad (7)$$

γ is the angle between \mathbf{k} and \mathbf{k}' . Surprisingly, this term σ_{xx}^a is proportional to n_i . Therefore, when n_i is small, we recover to the Boltzmann conductivity (5), but when n_i is large or $k_F \rightarrow 0$, which is usually interpreted as no “free carriers”, the Boltzmann term vanishes and the anomalous term σ_{xx}^a dominates. Since the spin polarization is proportional to the charge current density at the TI surface, this result also indicates another spin generation mechanism whose efficiency increases with n_i .

To have a glance of the physical origin of the anomalous conductivity, we start from an ideal system free of scattering and see how electronic states evolve under an external electric field \mathbf{E} . As shown in Figure 1a, when \mathbf{E} is applied to the system, all electronic states are going to drift in \mathbf{k} -space. After a time t , a state at point \mathbf{k} gains a displacement $\Delta\mathbf{k} = -e\mathbf{E}t/\hbar$. Yet \mathbf{E} cannot alter the spin orientation, so the spin stays at its original direction $\boldsymbol{\sigma}' = \boldsymbol{\sigma}$. However, due to the spin-momentum lock-up, the local energy eigenstate at \mathbf{k}' requires the spin be along \mathbf{k}' . Thus $\boldsymbol{\sigma}'$ is not the energy eigenstate at point \mathbf{k}' and is going to precess about \mathbf{k}' , which acts like an effective magnetic field \mathbf{B}_{eff} . The precession angular velocity is given by $\omega = 2v_F k' \approx 2v_F k$ in the limit of a weak field \mathbf{E} .

Therefore, an arbitrary spin orientation is not conserved on the surface of a 3D TI, unless it coincides with the local energy eigenstate. If, however, the time scale of interest is much shorter than the period of precession $\pi/(v_F k)$ so the precessional effect can be ignored, then the calculation for the ideal scattering-free system yields a simple result for the current (see Supplementary Information for details)

$$j_x(t) \approx \frac{e^2 v_F E}{4\pi \hbar} K t \quad (8)$$

where K is a quantity on the order of the Brillouin zone size and is only determined by the crystal structure. Note that this expression is independent of the Fermi wave vector k_F , which indicates this is not the normal Boltzmann term and strongly implies that such conduction has a topological origin. In fact, as we shall see later, equation (8) can be simply derived based on a topological point of view. Yet for now, it is evident that if we can somehow keep the surface spin approximately conserved, an electric field will drive a surface current increasing linearly with time. Ultimately this current is going to saturate over time because of the spin precession. The saturation current depends on how long the spin is approximately conserved, or the spin relaxation time τ_s .

Enhancement of spin relaxation time by nonmagnetic scattering

In 1971, Dyakonov and Perel presented a spin relaxation mechanism in noncentrosymmetric semiconductors based on a model of precessional random walks of spins [15, 5]. The essential picture can be applied to a 3D TI. Briefly, nonmagnetic scattering cannot alter the spin orientation, but in the interval between two consecutive scatterings the spin can precess under the effective magnetic field. If the impurity density n_i on a 3D TI surface is sufficiently high, the momentum relaxation time τ can be comparable to or even shorter than the precession period $\pi/(v_F k)$ and the spin orientation is going to wander around in a Brownian-like motion, as illustrated in Figure 1b,c.

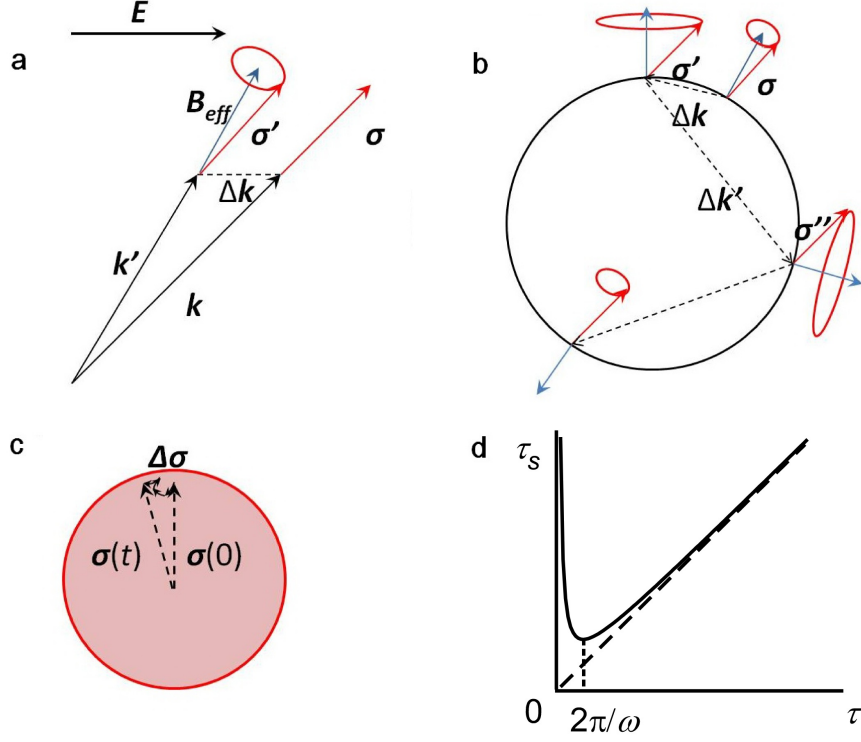


Figure 1: Spin relaxation time enhanced by nonmagnetic scattering. **a**, When an in-plane electric field \mathbf{E} is applied to the system, at time t the state at \mathbf{k} drifts to $\mathbf{k}' = \mathbf{k} + \Delta\mathbf{k}$, but the spin is unchanged ($\boldsymbol{\sigma}' = \boldsymbol{\sigma}$). Yet $\boldsymbol{\sigma}'$ is not the energy eigenstate at \mathbf{k}' and is going to precess about \mathbf{k}' which acts like an effective magnetic field \mathbf{B}_{eff} . **b**, The Dyakonov-Perel spin relaxation mechanism. Nonmagnetic scattering cannot alter spin, but during the interval of two consecutive scatterings, the spin precesses under the effective magnetic field caused by H_0 . Frequent nonmagnetic scattering, however, constantly changes the precession axis and makes the spin do a random walk on a unit sphere. **c**, The random walk of the spin slows down the spin relaxation and leads to a spin relaxation time τ_s inversely proportional to the scattering time or momentum relaxation time τ . **d**, The resultant enhancement of spin relaxation time τ_s when the scattering time τ is comparable or smaller than the precession period $2\pi/\omega$. The dashed line is for the “low-impurity” limit where the Dyakonov-Perel relaxation mechanism is not significant [14].

Based on this picture, if the number of Brownian motion steps in a given time t is $N = t/\tau$, the magnitude of the net spin displacement is $|\Delta\sigma| = \sqrt{N}\omega\tau = \omega\sqrt{\tau t}$. It is then clear that the time it takes to gain an appreciable spin displacement, i.e. the spin relaxation time τ_s is inversely proportional to τ , or proportional to n_i when $\tau \ll \pi/v_F k$, as shown in Figure 1d. Following (8) and replacing t with τ_s , the final current of the steady state is proportional to the impurity density $j_x \propto n_i$, which explains the result in (6).

To summarize why nonmagnetic scattering does not resist charge current but on the contrary enhances it, it is because the group velocity operator $\mathbf{v} = (1/\hbar)\partial H_0/\partial \mathbf{k}$ on the surface of a TI is determined by the spin only, unlike in a normal conductor where the group velocity is proportional to the momentum. Nonmagnetic scattering cannot change spin and thus has no resistance against the current. On the other hand, nonmagnetic scattering suppresses spin relaxation, and hence enhances the surface conductivity.

Band topology induced spin generation

The above Dyakonov-Perel mechanism satisfactorily explains how nonmagnetic scattering helps protect the spin from fast relaxation caused by precession. However, it does not describe how spins are generated in the first place. After all, the Hamiltonian of an electric field is also “nonmagnetic”, just as the nonmagnetic scattering term, and should not have the ability to alter the spin orientation. Interestingly, the answer lies in the unique topological nature of the surface band structure.

As widely known, the band structure at a 3D TI surface is a Dirac cone. Yet this linear dispersion only exists within a certain range about the Γ point in k-space, as illustrated in Figure 2b. As \mathbf{k} approaches the Brillouin zone boundary, these surface bands merge into bulk bands and their wave functions are no longer localized on the surface. Roughly, the size of the region where states are truly localized on the surface is noted as K , which has already appeared in equation (8). At the Brillouin zone boundary, energy bands must be continuous so as to form a periodic function in k-space. However, we immediately realize that a connection of these bands to themselves at the zone boundary is forbidden, because the wave functions at opposite sides of the Brillouin zone have opposite spin polarization. The solution to this dilemma is that these surface bands do not connect to themselves but to an identical Dirac cone on the opposite surface of the bulk. The two Dirac cones on the top and bottom surfaces of the bulk have opposite spin configurations thus allowing them to connect to each other in a correct way. Such topology is distinctively different from a normal band which connects to itself at the Brillouin zone boundary.

Under the influence of an electric field, all states are going to drift accordingly. As seen in Figure 2a, on the top surface, some “spin-right” surface states evolve out of the “surface state region” into bulk states and through the Brillouin zone boundary finally get to the “surface state region” on the bottom surface. Vice versa, some “spin-left” surface states on the bottom surface ultimately evolve onto the top surface. In short, an electric field does not directly change the spin but induces a pure spin current between the two surfaces through the bulk. This is not surprising in fact because the bulk of a topological insulator is a quantum spin Hall system in nature [16]. An electric field in a quantum spin Hall system is destined to induce a spin current which spatially separates different spins and causes spin accumulation on the two surfaces. If by a certain mechanism, e.g. the Dyakonov-Perel relaxation, the spins are (approximately) conserved, they will eventually build up on the surface and contribute to a spin-polarized charge current which increases linearly with time.

Let’s see if we can obtain a result of the charge current based on this topological point of view. As shown in Figure 2c, at time t , all states are to gain a displacement $\Delta k = eEt/\hbar$. At angle θ , the number of states which move out of the “surface state region” is $\Delta k \cos\theta K d\theta/(2\pi)^2$. Multiplying a factor $\cos\theta$ for obtaining the x-component of spin and integrating over the circle, we can calculate the total spin accumulated within time t . Based on relation (2), the charge current can then be derived as following.

$$\begin{aligned} j_x(t) &= \int_0^{2\pi} \frac{eE}{\hbar} t \cos\theta K d\theta \cdot \frac{1}{(2\pi)^2} \cdot \cos\theta \cdot ev_F \\ &= \frac{e^2 v_F E}{4\pi\hbar} K t \end{aligned} \quad (9)$$

which is exactly the same as we obtained in (8). Since this derivation involves nothing about the occupancy of the surface bands (as long as it’s within the surface state region $k_F < K$), the result is certainly independent of k_F . The above calculation further quantitatively confirms the physical picture of spin transport between the two surfaces.

It is worth noting that the same picture can be applied to 2D TIs, and is able to reproduce the result of the well known dissipationless charge transport. (See Supplementary Information for details.)

Comparison to other 2D systems with similar band structure

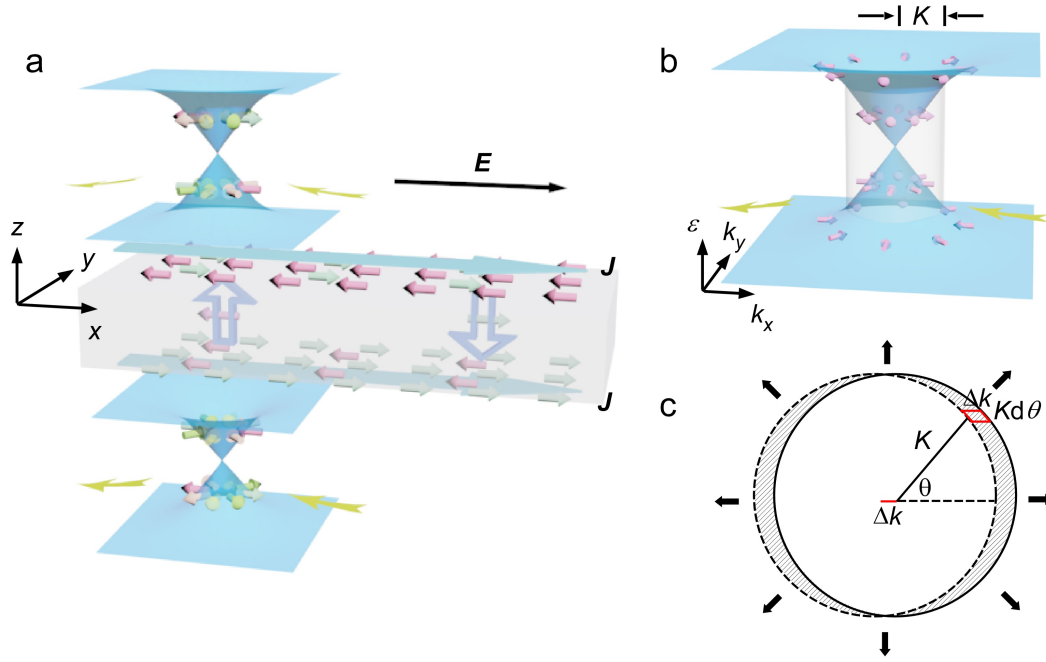


Figure 2: Spin generation caused by an in-plane electric field on a 3D TI surface. **a**, The top and bottom surfaces of a 3D TI each contain a Dirac cone with identical dispersion but opposite spin configuration. At the Brillouin zone boundary, these two cones connect with each other forming a topology inequivalent to a normal band. Due to such a topological band structure, an in-plane electric field can separate different spins and cause spin accumulation on the two surfaces and this results in a charge current. The small cylindrical arrows indicate spin orientation. The hollowed vertical arrows indicate spin current. The long horizontal blue arrows indicate charge current. The yellow arrows indicate the direction of state drift caused by the electric field. **b**, The band structure of the top surface. The shaded box indicates the region in k -space where the electronic states are truly localized on the surface, while out of the box the electronic states are extensive in the bulk. The radius of this region is K . Driven by an electric field, some “spin-left” bulk states drift to the surface on the right side of the box while some “spin-right” surface states drift to the bulk on the left side of the box. A similar process is happening on the bottom surface as well. **c**, Calculation of the total spin injected onto the top surface during a time t . The shaded area denotes electronic states entering/exiting the surface region. The small solid arrows indicate spin orientation.

It is instructive to compare the 2D surface of a 3D TI to other 2D systems with a similar linear dispersion such as graphene and 2DEG with a Rashba-like spin splitting. Indeed, the Dyakonov-Perel spin relaxation mechanism is not unique in 3D TIs, but also existent in graphene and 2DEG. However, we will show below that the above spin generation mechanism is unique to 3D TIs and is absent in other 2D system with trivial topology.

The distinction from graphene is simple to address. First, the observed long spin relaxation time in graphene caused by Dyakonov-Perel scattering [17, 18] is for the real spin of electrons rather than the pseudo-spin coupled to the momentum in H_0 . While on a 3D TI surface the pseudo-spin highly matches the real spin, in graphene they are two completely independent degrees of freedom and have no direct relation at all. Thus the prolonged spin relaxation time in graphene is not manifested in conductivity. Second, the pseudo-spin relaxation in graphene greatly suffers from the inter-valley scattering by impurities which causes a reduction in this anomalous conductivity, but each surface of a 3D TI only contains one Dirac cone and is free of such effect.

2DEG, however, deserves more insights. The velocity operator in 2DEG is $\mathbf{v} = \mathbf{p}/m + \lambda\boldsymbol{\sigma} \times \mathbf{n}$ where the second spin term is only a small correction. A direct comparison in conductivity is thus inappropriate. However, even if we only look at the induced spin accumulation in 3D TIs and 2DEGs, the results are still qualitatively different. Calculation in [19] shows that in a 2DEG with Rashba splitting, the spin accumulation S^y induced by an in-plane electric field is proportional to the scattering time τ instead of τ_s even in the scenario of Dyakonov-Perel relaxation mechanism. This implies that something on the surface of a 3D TI is fundamentally different from a 2DEG with Rashba splitting.

To see this point more clearly, we compare the band structures of the two systems, as shown in Figure 3 a,b. Though both contain a singularity at the Γ point, the band structure of a 2DEG is topologically inequivalent to a 3D TI. In a 2DEG, the quadratic \mathbf{k}^2 term in the Hamiltonian bends up both two bands at large \mathbf{k} so that the Fermi level intersects both bands. Such a system essentially involves no physics at the Brillouin zone boundary. We can perform a topological transformation to the band structure of a 2DEG to resemble that of a 3D TI surface, as shown in Figure 3c. After this transformation, we end up with two ‘‘Fermi levels’’ – one is an upper bound ϵ_{F1} , the other is a lower bound ϵ_{F2} . The occupied states are those between them. It is simple to apply our calculation to such an imagined auxiliary system, and a result of no spin accumulation is obtained in the limit of $\tau \rightarrow 0$ (or $\tau_s \rightarrow \infty$) – just as expected for the 2DEG system. The details of the calculation can be found in the Supplementary Information.

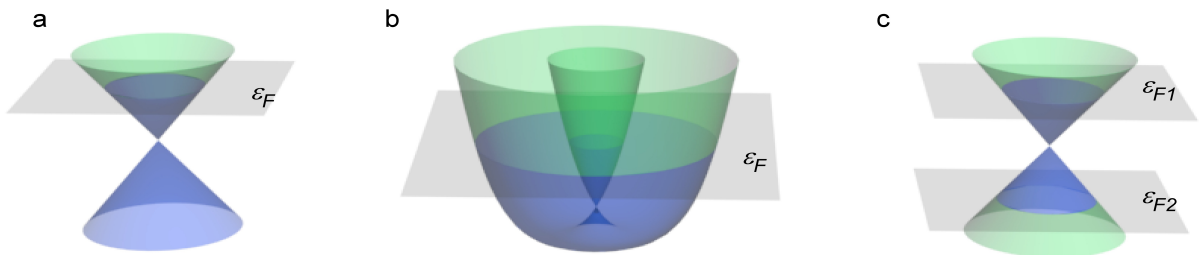


Figure 3: The spin generation mechanism originates from the band topology rather than the detailed energy dispersion. The blue area denotes occupied states and the green area denotes unoccupied states. **a**, The energy band of a 3D TI surface where all states below the Fermi level ϵ_F are occupied. The Fermi level intersects only one of the two branches of the energy band. **b**, The energy band of a 2DEG with Rashba-like spin splitting. The Fermi level intersects both branches of the energy band. **c**, An imagined system with the same shape of dispersion as **a** but is topologically equivalent to **b** rather than **a**. The occupied states are those between ϵ_{F1} and ϵ_{F2} . Calculation for such a system yields a result same as **b** (no spin generation in the limit of $\tau_s \rightarrow \infty$) rather than **a** (finite spin generation rate in the limit of $\tau_s \rightarrow \infty$).

Experimental evidence

Field effect measurements in TIs have often shown a high minimum conductivity even when the Fermi level is tuned to the Dirac point by gate voltage and “free carriers” are completely depleted [9, 10, 11, 12]. The reported minimum surface conductivity varies from sample to sample and ranges from 5 to $50e^2/h$. To date, two possible mechanisms, bulk impurity bands [10] and surface electron puddles [11], have been proposed to explain this conductivity residue. However, neither mechanism can explain the experimental observations satisfactorily (details in Supplementary Information), which implies the existence of an anomalous conductivity component as predicted by our theory. Quantitative comparison between our theory and pre-existing experiment is challenging, because of the unknown scattering term. The k_F dependence of σ_{xx}^a in (6) involves the detailed form of the scattering potential. For screened charge impurities such as Se vacancies, the calculated conductivity σ_{xx}^a has a $1/k_F^2$ divergence at $k_F = 0$. This non-physical divergence originates from the absence of screening when carrier concentration $n \rightarrow 0$. Under the unscreened, long-range Coulomb potential, the TI surface becomes a strongly correlated system. As a result, electron/hole puddles can be formed and the crystal momentum \mathbf{k} becomes ill-defined [20]. A more rigorous non-perturbative treatment of the scattering term is therefore required. Furthermore, the nature of the scattering is unclear as the surface defects may be created when exposed to air [11, 21]. If the scattering is short-ranged, the calculation gives a logarithmic divergence in k_F which is much weaker than screened charges.

Though a clear identification of the surface impurity composition and a more rigorous non-perturbative method are necessary to quantify the Fermi level dependence of the surface conductivity, some non-monotonic behavior of the conductivity with anomalous increase near the Dirac point is implied by our theory. Amazingly, such effects have been observed experimentally: the gate voltage dependent conductivity measurement of Bi_2Se_3 has often shown “kinks” [22] or non-monotonic “tails” [11, 12], as opposed to similar measurements in graphene or normal semiconductors. These experimental observations are not yet understood. A more clear conductivity “bump” near the Dirac point has been observed by ourselves in a considerable amount of devices, when tuning the Fermi level of Sb-doped Bi_2Se_3 nanoplates by gate voltage, as shown in Figure 4. The single crystalline Bi_2Se_3 nanoplates are grown by chemical vapor deposition (CVD) with their Fermi levels carefully tuned within the bulk band gap by controlling the amount of dopants [22].

Further experiments can be carried out to confirm our theory. The most distinctive prediction by our theory is that at a fixed Fermi level position, the anomalous conductivity is proportional to the impurity density n_i . Techniques such as ion implantation or surface impurity coating may be used to control the surface impurity density to test this prediction. More detailed physical modeling and numerical simulation can be used to determine the nature of the surface scattering, in comparison with the experimental results.

In summary, our theory reveals an efficient spin generation mechanism in a 3D TI. The topological nature of the band structures at the TI surface demands a pure bulk spin current between the opposite surfaces. Nonmagnetic scattering can enhance spin relaxation time, allowing substantial spin accumulation at the surfaces of a 3D TI with high impurity density. Our theory is supported by the experimental observations of high conductivity at the Dirac point. Importantly, this discovery not only provides valuable fundamental physical insights on controlling spin/charge transport in 3D TIs, but also offers a new and practical method for the enhancement of surface spin polarization by harnessing the nonmagnetic impurities.

Methods

For the calculation, we use the density matrix approach so as to allow for an ensemble treatment of the scattering. The method is similar to that in [8] except for no assumption of a small n_i . The quantum Liouville equation for the density matrix ρ is

$$\frac{d\rho}{dt} + \frac{1}{i\hbar}[\rho, H] = 0 \quad (10)$$

The commutators of ρ with the three terms in H are evaluated respectively. In calculation, the first-order Born approximation is used for the scattering term U and the electrostatic driving term $e\mathbf{E}\cdot\mathbf{r}$. The impurities are assumed nonmagnetic and uncorrelated so that the average of $\langle \mathbf{k}s|\hat{U}|\mathbf{k}'s'\rangle\langle \mathbf{k}'s'|\hat{U}|\mathbf{k}s\rangle$ over impurity configuration is replaced by $n_i|\bar{U}_{\mathbf{k}\mathbf{k}'}|^2\delta_{ss'}/V$ where n_i is the impurity density, V is the volume and $\bar{U}_{\mathbf{k}\mathbf{k}'}$ is the matrix element of the potential of a single impurity. Under a weak electric field \mathbf{E} , the density matrix ρ in the electrostatic driving term is replaced by the equilibrium state version ρ_0 . No such treatment is performed on the scattering term U , to ensure the accuracy in case of a relatively high n_i . Under all these assumptions, we end up with a set of linear kinetic equations from which the density matrix ρ can be directly obtained. Physical quantities such as the spin density $\boldsymbol{\sigma}$ and charge current \mathbf{j} can then be calculated.

Experimentally, Sb-doped Bi_2Se_3 nanoplates were synthesized in a tube furnace (Lindberg Blue M) via a CVD method similar to [22]. Briefly, Bi_2Se_3 , Sb and Se powders were employed as precursors and Au thin films (20 nm) served as the catalyst. The excess Se powder ensured a Se-rich environment for the growth. By carefully adjusting the mass ratio of Bi_2Se_3 and Sb, we were able to control the doping concentration to a desired range. The as-grown nanoplates were then transferred onto 300 nm SiO_2 -covered, heavily-doped p-type Si substrates. Subsequently, top electrical contacts (100 nm Au / 100 nm Cr) were defined using electron beam lithography. The two top contacts functioned as source and drain electrodes, while the Si substrate served as the back gate.

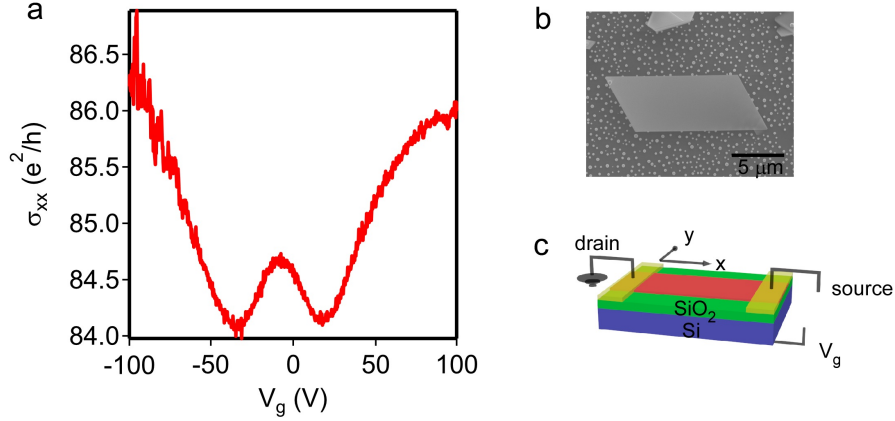


Figure 4: Experimental evidence supporting the anomalous conductivity. **a**, Longitudinal conductivity as a function of gate voltage for a 100 nm-thick Sb-doped Bi_2Se_3 plate at 79 K. As opposed to a normal V-shape curve, this sample showed two conductivity valleys separated by a peak. Such double-valley behavior has been observed in a considerable amount of samples, though not universally existent in all samples. **b**, The scanning electron microscopic (SEM) image of a typical as-grown Sb-doped Bi_2Se_3 plate by CVD. The scale bar denotes 5 μm . **c**, A schematic diagram of the device. The actual geometry of the device in **a** was 6.6 μm (channel length) \times 2.8 μm (channel width) \times 100 nm(thickness).

Acknowledgement

The authors thank Jesse Taing and Nima Maghoul for the sample preparation; Shu-Ting Pi, Mark Triplett and Amanda Parker for extensive discussions; Prof. Nicholas Curro and Adam Dioguardi for the assistance in low-temperature measurement; Xi Chen for the 3D visualization. This work was supported by the U.S. National Science Foundation Grant DMR-1310678.

Author contributions

X.P. built up the theoretical model and performed calculations. X.P. and Y.Y. carried out the experimental measurements in the laboratory of D.Y. All authors participated in scientific discussions and manuscript preparation.

Additional information

Details of calculation, experimental discussion and further comparison to 2D TIs can be found in Supplementary Information. Supplementary information is available in the online version of the paper. Reprints and permissions information is available online at www.nature.com/reprints. Correspondence and request for materials should be made to D.Y.

Competing financial interest

The authors declare no competing financial interest.

References:

- [1] Hasan, M. Z. & Kane, C. L. Colloquium: Topological insulators. *Rev. Mod. Phys.* **82**, 3045-3067 (2010).
- [2] Zhang, H. J. et al. Topological insulators in Bi_2Se_3 , Bi_2Te_3 and Sb_2Te_3 with a single Dirac cone on the surface. *Nat. Phys.* **5**, 438-442 (2009).
- [3] Chen, Y. L. et al. Experimental realization of a three-dimensional topological insulator, Bi_2Te_3 . *Science* **325**, 178-181 (2009).
- [4] Konig, M. et al. Quantum spin Hall insulator state in HgTe quantum wells. *Science* **318**, 766-770 (2007).
- [5] Pesin, D. & MacDonald, A. H. Spintronics and pseudospintronics in graphene and topological insulators. *Nat. Mater.* **11**, 409-416 (2012).
- [6] Li, C. H. et al. Electrical detection of charge-current-induced spin polarization due to spin-momentum locking in Bi_2Se_3 . *Nat. Nanotechnol.* **9**, 218-224 (2014).
- [7] Bernevig, B. A., Hughes, T. L. & Zhang, S. C. Quantum spin Hall effect and topological phase transition in HgTe quantum wells. *Science* **314**, 1757-1761 (2006).
- [8] Culcer, D., Hwang, E. H., Stanescu, T. D. & Das Sarma, S. Two-dimensional surface charge transport in topological insulators. *Phys. Rev. B* **82**, 155457 (2010).
- [9] Checkelsky, J. G., Hor, Y. S., Cava, R. J. & Ong, N. P. Bulk band gap and surface state conduction observed in voltage-tuned crystals of the topological insulator Bi_2Se_3 . *Phys. Rev. Lett.* **106**, 4 (2011).
- [10] Sacepe, B. et al. Gate-tuned normal and superconducting transport at the surface of a topological insulator. *Nat. Commun.* **2**, 7 (2011).
- [11] Kim, D. et al. Surface conduction of topological Dirac electrons in bulk insulating Bi_2Se_3 . *Nat. Phys.* **8**, 459-463 (2012).
- [12] Steinberg, H., Gardner, D. R., Lee, Y. S. & Jarillo-Herrero, P. Surface state transport and ambipolar electric field effect in Bi_2Se_3 nanodevices. *Nano Lett.* **10**, 5032-5036 (2010).
- [13] Shen, S.-Q. *Topological insulators: Dirac Equation in Condensed Matters*. 25 (Springer, 2012).
- [14] Xin, L. & Sinova, J. Reading charge transport from the spin dynamics on the surface of a topological insulator. *Phys. Rev. Lett.* **111**, 166801 (166805 pp.)-166801 (166805 pp.) (2013).
- [15] Dyakonov, M. I. & Perel, V. I. Spin relaxation of conduction electrons in noncentrosymmetric semiconductors. *Soviet Physics: Solid State, USSR* **13**, 3023-3026 (1972).
- [16] Hasan, M. Z. & Moore, J. E. Three-dimensional topological insulators. *Annu. Rev. Condens. Matter Phys.*, **2**, 55-78 (2011).
- [17] Han, W. & Kawakami, R. K. Spin relaxation in single-layer and bilayer graphene. *Phys. Rev. Lett.* **107**, 4 (2011).
- [18] Yang, T. Y. et al. Observation of long spin-relaxation times in bilayer graphene at room temperature. *Phys. Rev. Lett.* **107**, 4 (2011).
- [19] Mishchenko, E. G., Shytov, A. V. & Halperin, B. I. Spin current and polarization in impure two-dimensional electron systems with spin-orbit coupling. *Phys. Rev. Lett.* **93**, 4 (2004).
- [20] Beidenkopf, H. et al. Spatial fluctuations of helical Dirac fermions on the surface of topological insulators. *Nat. Phys.* **7**, 939-943 (2011).
- [21] Park, S. R. et al. Quasiparticle scattering and the protected nature of the topological states in a parent topological insulator Bi_2Se_3 . *Phys. Rev. B* **81**, 4 (2010).
- [22] Seung Sae, H., Cha, J. J., Desheng, K. & Yi, C. Ultra-low carrier concentration and surface-dominant transport in antimony-doped Bi_2Se_3 topological insulator nanoribbons. *Nat. Commun.* **3**, 757 (757 pp.)-757 (757 pp.) (2012).